LAWRENCE
LIVERMORE
NATIONAL
LABORATORY

LLNL-JRNL-865630

# Multichannel Doppler fiber-imager spectrometer for spatio-temporal characterization of high-intensity laser-driven plasmas

G. Zeraouli, M. Marconi, B. Sullivan, S. Wang, S. Zahedpour Anaraki, R. Hollinger, S. Shlyaptsev, D. A. Mariscal, J. J. Rocca

June 15, 2024

Review of Scientific Instruments

## Disclaimer

This document was prepared as an account of work sponsored by an agency of the United States government. Neither the United States government nor Lawrence Livermore National Security, LLC, nor any of their employees makes any warranty, expressed or implied, or assumes any legal liability or responsibility for the accuracy, completeness, or usefulness of any information, apparatus, product, or process disclosed, or represents that its use would not infringe privately owned rights. Reference herein to any specific commercial product, process, or service by trade name, trademark, manufacturer, or otherwise does not necessarily constitute or imply its endorsement, recommendation, or favoring by the United States government or Lawrence Livermore National Security, LLC. The views and opinions of authors expressed herein do not necessarily state or reflect those of the United States government or Lawrence Livermore National Security, LLC, and shall not be used for advertising or product endorsement purposes.

LLNL-JRNL-865630

# Multichannel Doppler fiber-imager spectrometer for spatio-temporal characterization of high-intensity laser-driven plasmas

G. Zeraouli,[1, 2, a)] M. Marconi,[1] B. Sullivan,[1, 3] S. Wang,[1] S. Zahedpour Anaraki,[1] R. Hollinger,[1] S. Shlyaptsev,[1] D. Mariscal,[2] and J. J. Rocca[1, 3]

[1)] *Colorado State University, Fort Collins CO 80523, USA*

[2)] *Lawrence Livermore National Laboratory, Livermore CA 94550, USA*

[3)] *XUV Lasers, Fort Collins, CO, 80523, USA*

(Dated: 27 December 2023)

We demonstrate a flexible multichannel fiber-based imaging Doppler spectrometer to characterize plasmas in high intensity ($\geq 1\times10^{18}$ W/cm$^2$) laser-plasma experiments at high repetition rate. The instrument collects data from $\times21$ different plasma locations combining optical fibers and a single imaging spectrometer. This diagnostic maps the plasma velocity evolution as a function of time with sub-pico-second resolution. Experimental results showing 2D velocity measurements of an expanding plasma with 20 $\mu$m spatial resolution are presented. Intensities of the order of $10^{18}$ W/cm$^2$ were used to generate an expanding plasma while a much less intense, frequency doubled (400 nm), probe beam ($10^{11}$ W/cm$^2$) was used to measure the Doppler shift from the plasma critical surface. The instrument can be scaled to a larger number of channels (e.g. 100).

## I. INTRODUCTION

The interaction of ultra-intense laser pulses from the rapidly increasing number of ultra-fast petawatt class lasers[1] with solid targets creates extreme environments[2–4] and drives relativistic phenomena.[5,6] Impactful outcomes include bright sources of x-ray radiation[7,8] and beams of high energy particles[9,10] for applications such as fusion energy[11,12], ultra-fast radiography of large dense objects (e.g. airplane turbines in motion)[13], material science[14] and medicine[15], motivates seeking an increased understanding of these interactions. Direct measurements of relevant plasma properties, such as velocity, density, and temperature, can provide fundamental information to control the generation of high-intensity secondary laser sources and expand applications.

A range of different instruments have been developed to measure plasma velocity. The VISAR[16,17] (velocity interferometer system for any reflection) is one of the most widely used and reliable diagnostics for such applications. Spatial resolution of a few microns have been experimentally achieved using the VISAR. However, its time resolution is typically on the order of several tens of picoseconds to nanoseconds. This makes it challenging to map the velocity of a rapidly expanding high intensity-driven plasma in the transverse direction with a high temporal resolution. Alternatively Doppler shift-based spectroscopy is a robust and well understood technique which has been used to characterize rapidly evolving processes[18–20]. Recently the principle has been successfully applied to characterize the 2D ultra-fast laser-driven plasma dynamics[21,22] (with velocities of the order of $10^5$ m/s) using a set of 16 spectrometers. Enhancing the spatial resolution of these measurements would help to unravel the dynamics of the critical density in the picosecond time scale and better describe the related laser absorption, plasma instabilities and acceleration mechanisms.

[a)]The author to whom correspondence may be addressed: Ghassan.Zeraouli@Colostate.edu

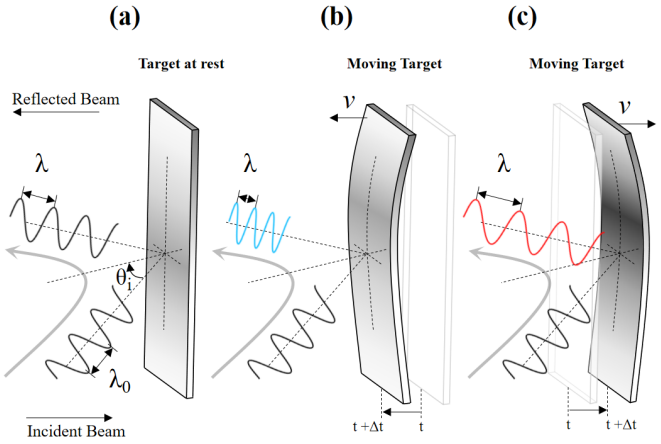


FIG. 1. (a) Incident probe beam at angle $\theta$ and wavelength $\lambda_0$ interacting with a target at rest. (b)(c) Doppler shift effects on the probe beam depending on the direction of reflective surface displacement.

Here we present a Doppler shift spectroscopy multi-channel instrument that uses the combination of fibers and a single imaging spectrometer to records maps of the spatio-temporal evolution of high intensity laser driven plasmas at 21 locations with high repetition-rate (HRR) capabilities. The design and development of the new flexible instrument together with a demonstration of its use in diagnosing evolving high-intensity laser-driven plasmas (recording velocities up to $10^6$ m/s) are presented.

## II. DOPPLER SHIFT SPECTROSCOPY PRINCIPLE AND PARAMETER DEFINITION

Consider a perfectly flat target at rest (Fig.1.a). Suppose also that the target acts as a mirror for an incident probe beam with a central wavelength $\lambda_0$ impinging at an angle $\theta$ (to the normal axis). When the target is at rest, the reflected probe beam wavelength $\lambda$ is equal to $\lambda_0$ (see Fig.1.a).

When the target (mirror) moves at a speed $v$ (to the left as in Fig.1.b or to the right as in Fig.1.c), the wavelength of the reflected beam $\lambda$ is shifted from $\lambda_0$. If the target displacement is contrary to the direction of the incident probe beam (Fig.1.b), $\lambda_0$ experiences a "blue shift". In the opposite situation (Fig.1.c), $\lambda$ shifts to longer wavelengths, leading to a "red shift". The velocity dependent relation between $\lambda_0$ and $\lambda$ is given by[23]:

$$\frac{\lambda}{\lambda_0} = \frac{1-\frac{v^2}{c^2}}{1-2\frac{v}{c}\cos\theta+\frac{v^2}{c^2}} \quad (1)$$

This relation permits to estimate the velocity $v$ of the moving target by measuring the wavelength shift $\Delta\lambda$ where $\Delta\lambda = \lambda - \lambda_0$. In the non relativistic case ($v<<c$), we can simply write:

$$v = \frac{c}{2}\left(\frac{\Delta\lambda}{\lambda_0}\right) \quad (2)$$

To perform successful Doppler shift measurements, a well characterized probe beam wavelength is needed, while a high resolution optical spectrometer is needed to measure the spectrally shifted probe beam.

## III. THE FIBER-IMAGER SPECTROMTER

### A. Working principle

The flexible multichannel Fiber-Imager SpectromtER (FISER) described here is illustrated in Fig.2. It consists of two main components. The first is a set of $\times 21$ graded index multi-mode optical fibers (Thorlabs GIF625-100, 62.5 $\mu$m core diameter) spread within a circle of $\sim$500 $\mu$m radius. Its purpose is to transport the collected light to the instrument input ($\sim$1 m away) and to convert the 2D fiber distribution at the fiber bundle input (Fig.3.a) into a 1D distribution at the fiber output (Fig.3.b). The second component is a tunable Czerny-Tuner imaging spectrometer. The linear output of the fiber bundle serves as the slit of the spectrometer. The spectrally resolved image is then collected at the output of the spectrometer by a 12 Bit Quantalux monochrome sCMOS camera (Thorlabs CC215MU), placed at the output of the imaging spectrometer. The image is then processed and analyzed to generate 2D resolved velocity map of the plasma as a function of delay between the pump and probe beams. Acquisition at different delays maps the full spatio-temporal evolution of the plasma.

### B. Spectral calibration

We spectrally calibrated the FISER using a mercury (Hg) lamp emitting two spectral lines at 407.7nm and 404.6nm. These Mercury line emissions were used to convert the distance in pixels on the camera to wavelength. A diode laser, emitting at 405 nm, was also used to cross-check the spectral calibration.

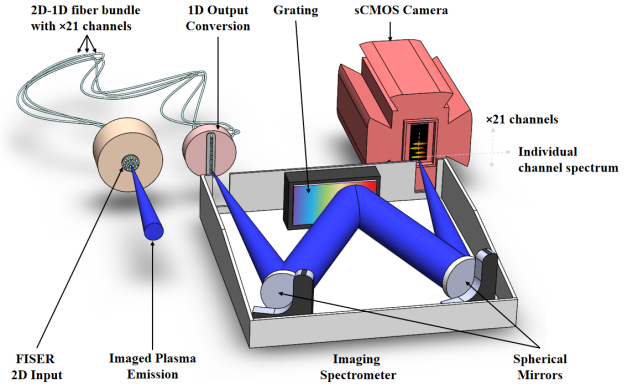


FIG. 2. 3D structure of the FISER diagnostic.

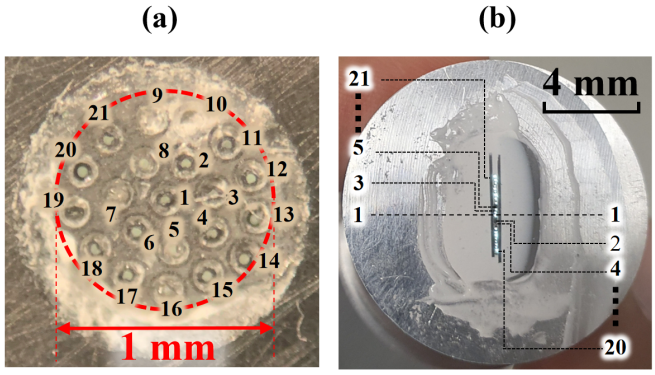


FIG. 3. (a) Microscopic view of the FISER 2D input with the fiber numbering. (b) Output of the fiber converting the 2D distribution onto 1D. Pair fiber numbers were distributed on one side, while the impairs on the other.

Fig.4.a shows images acquired on the sCMOS camera for the two calibration light sources used. It shows the spectra collected by each of the fibers (distributed on the horizontal direction) using the mercury lamp (top) and the laser diode (bottom). Fig.4.b shows the spectral lineouts for the three light sources for one of the channels. The resulting estimated spectral resolution of the instrument is $\Delta\lambda/\lambda$=6.5$\times 10^{-4}$. Performing these tests permitted also to define the sign of the Doppler shift. The red shift corresponds to a wavelength shift towards the the top of the image, while the blue shift corresponds to a shift towards the bottom.

## IV. EXPERIMENTAL DEMONSTRATION OF THE INSTRUMENT

The main goal of the experiment was to demonstrate the FISER by measuring the spatio-temporal evolution of a high-intensity laser-driven. Fig.5 represents the scheme of the experiment used to generate and probe the plasma at ALEPH[24] laser.

An intensity of the order of $1.6\times 10^{18}$ W/cm$^2$ was used to create an expanding plasma focusing the compressed (50 fs) high energy (4 J) pulses onto a 57 microns focal spot using a

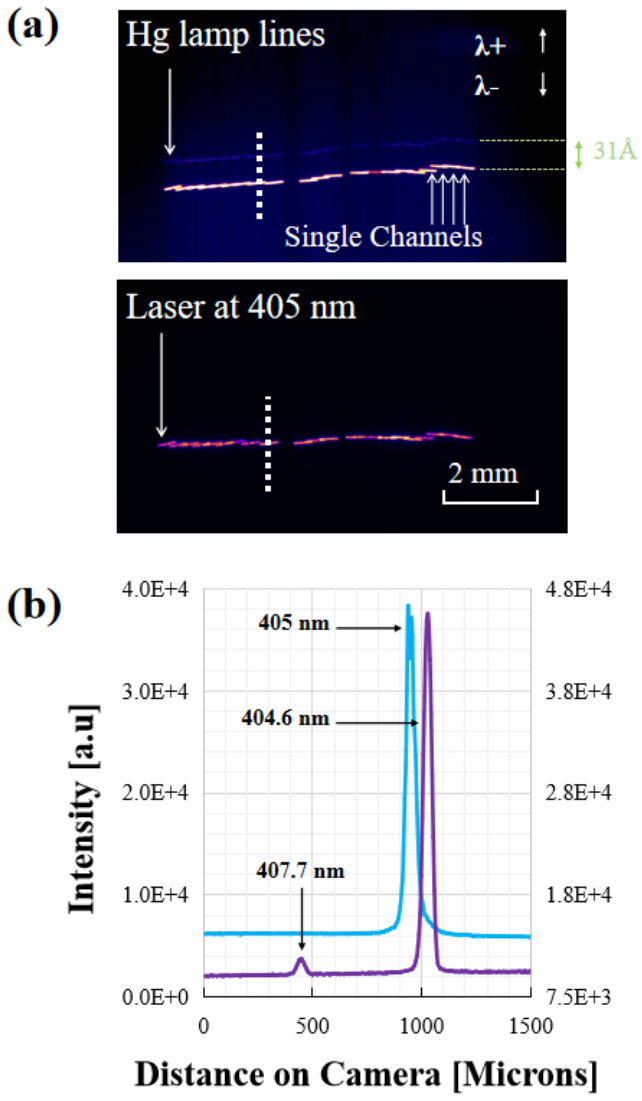


FIG. 4. (a) Experimental results for the spectral calibration of the FISER using a Hg lamp (Top) and a laser diode (bottom). (b) Signal profiles from the two light sources collected on the sCMOS camera for channel 4.

long focal length parabola (F/25). A flat glass ($SiO_2$) target was used. A low energy (100 $\mu$J) frequency doubled probe beam with 50 fs pulses was focused onto a 66 microns. We note that the probe and pump beams have orthogonal polarization. A high magnification imaging system (M=10) was built to image both the plasma and the frequency shifted probe beam onto the FISER (placed 2 meters away from the interaction). Moving a delay stage (see Fig.5) allows one to perform velocity measurements at different plasma expansion times. For this experiment we scanned delays between 1 ps to 10 ps. Finally, note that we performed the experiment at intensity levels where the second harmonic signal generated by the plasma is insignificant compared to the signal from the probe beam used for the Doppler shift measurements.

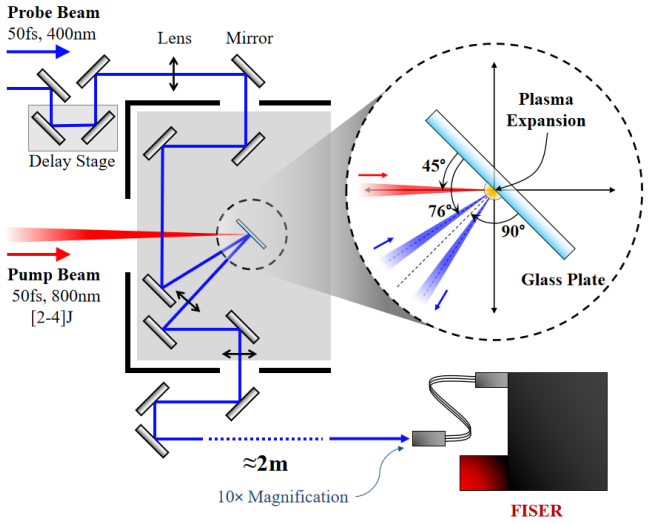


FIG. 5. Experimental setup for the spatio-temporal velocity mapping of laser-driven hot plasma performed at ALEPH.

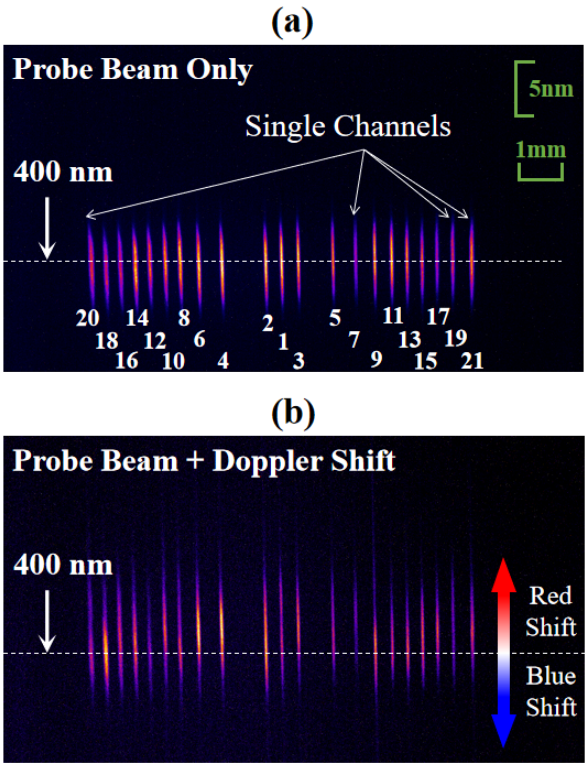


FIG. 6. (a) Measured probe beam spectrum on each of the optical fibers before the interaction. (b) Example of measured spectrum (Doppler shifted probe beam) a few picoseconds after the interaction.

## V. RESULTS AND DISCUSSION

Fig.6 presents two sets of spectra obtained with and without a plasma.

Fig.6.a shows spectra corresponding to 21 position in the

probe beam with no plasma present. The numbers identify the location of the fibers at the fiber holder input (see Fig.3), i.e. different position on the plasma. Fig.6.b shows an example of a Doppler shifted probe beam after the interaction with the dynamic plasma. The dashed white line refers to the initial probe beam central wavelength, $\lambda_0$=400 nm. We can clearly see in Fig.6.b the spectral broadening and the shift of the probe beam on the vertical direction (red shift) indicating the Doppler effect a few picoseconds after the interaction.

Based on Eq.2 and knowing the spatial distribution of the fibers (Fig.3), it is possible to reconstruct the spatio-temporal evolution of the plasma by varying the delay between the pump and probe beams as shown in Fig.7.

Fig.7.a shows the results of the 2D Doppler shift analysis for pump-to-probe delays between 1 ps to 10 ps. Each of the circles represents a single fiber at its physical location relative to the imaged plasma and is obtained by averaging the signal over three shots per delay. The color of each fiber refers to the plasma velocity calculated using Eq.2 as a function of delay. We note that 0 ps delay indicates the time at which both pump and probe beams are temporally overlapped. We also note that we couldn't measure the velocity on channel 16 because of the very low signal-to-noise ratio at that location. This ratio mainly depends on the plasma dynamics on each shot, which depends itself on the laser irradiation intensity, target roughness, local parametric instabilities and the delay at which the measurements are carried out. We also note that the spatial resolution of the system is determined by the magnification of the optical system used to image the plasma at the entrance of the instrument, the core diameter of the optical fibers used and the separation between the fibers. In the case of the instrument presented here the magnification was 10 and the spatial resolution is estimated to be 20 $\mu$m on the plasma surface. Fig.7.b presents the reconstructed error map for the probe beam only (measured without pump beam, i.e. with no plasma). The error map quantifies the probe beam spectral shift from shot-to-shot on new targets. These errors are mainly due to shot-to-shot target alignment and surface reflectivity fluctuations due to variation in surface roughness. We note that these errors (up to $\sim 2.5\times10^4$ m/s) are negligible compared with the spectral shifts induced by the plasma.

To understand the observed data we performed a series of PIC and hydro simulations conducted with the codes EPOCH[25] and RADEX[26] presented in Fig.8. The large focal spot, d$\sim$ 57 $\mu$m in diameter, and the close proximity of the critical density to the target surface, x < 3-8 $\mu$m, allowed us to simplify the simulation to 2D without deviating too far from reality. This is because at x/d $\ll$ 1 the multi-dimensional effects are still small and the expansion is almost planar. As a result, it was possible to perform the simulations in reasonable time and also include multi-dimensional effects which are important in understanding of spread of critical density speeds inside the focal spot.

Using the simulations in Fig.8, we calculated the velocity of the critical density front at different delays (Fig.8.a to h). We see the critical density front moves in the laser direction at high velocities (Fig.8.a to Fig.8.d) and peaks at $\sim 1\times10^6$m/s. Later, the critical density front is observed to decelerate up to 4 ps (Fig.8.e to g) after the interaction before starting to accelerate again in the opposite direction, 5 ps after the interaction (see Fig.8.h).

Fig.9 presents the measured plasma velocity as a function of delay averaged over all the diagnostic field of view region compared to two EPOCH calculations for two different pre-plasma scale lengths.

A significant red shift is observed between 1 ps to 2 ps after the interaction meaning that the critical density front is accelerating in the laser forward direction, before it starts to decrease. According to Fig.9, we can see that the velocity is no longer positive at 5 ps, which corresponds to a plasma expansion and movement of the critical surface in the opposite direction. The last point recorded at 10 ps after the interaction shows almost no shift, showing that this critical surface is no longer moving. Error bars represent the RMS velocity measured on 21 fibers for each delay, for up to three shots per delay. The experimental results presented in Fig.9 show reasonably good agreement with the EPOCH calculations when the pre-plasma is assume to have a scale length of 2 to 2.5 $\mu$m. This means that in addition to measuring the dynamics of the plasma few picoseconds after the interaction, the FISER measurements also provided information about the scale length of the pre-plasma.

An important conclusion from our simulations is that the plasma dynamics is strongly influenced by the presence of a pre-plasma. Agreement with the experimental data presented in Fig.9 requires the presence of a substantial amount of pre-plasma prior to the arrival of the main laser pulse. Fig.8 shows maps of the electron density for different times respect to the arrival of the laser pulse, assuming a contrast of $10^{-8}$ in the 1 ns prior to the main pulse, as measured for our laser. The heating pulse, impinging at 45 degrees, penetrates the pre-plasma until it reaches a density of $8.8\times10^{20}$ cm$^{-3}$ (corresponding to half the critical density), where it is refracted back. The associate change in momentum transfers into the plasma, creating a forward-propagating a high amplitude shock wave that causes a red shift of the probe beam (Fig.9). When the shock wave reaches the target, it is reflected back with a substantially reduced speed, which gives origin to the observed blue shift. If the plasma density gradient scale length ($L_{grad}$) were to be very small, $L_{grad}$ <1 $\mu$m, case corresponding to a high contrast laser, the shock wave would quickly reach the density where it is reflected back. In this case the simulations show a negative (blue) shift that would take place from the start, which we suspect is the case observed by a previous experiment**??**. On the contrary, if the gradient length were to be large, $L_{grad}$> 3-4 $\mu$m, then the shock wave would travel thought the increasing density ramp of the pre-plasma for too long, to reach the turning point of the $2\omega$ probing laser ($6.5\times10^{21}$ cm$^{-3}$ at the incidence angle of 14 degrees, almost the critical density). With even larger gradient scale lengths the shock magnitude would weakens after so much travel, and the maximum value of density reached would become lower than the corresponding to $2\omega$ critical density, which would turn to be undetectable by the probe laser. It's also interesting to notice that the simulated shape of shock wave is substantially distorted by the instabilities (see Fig.8). The exact nature of such instabilities

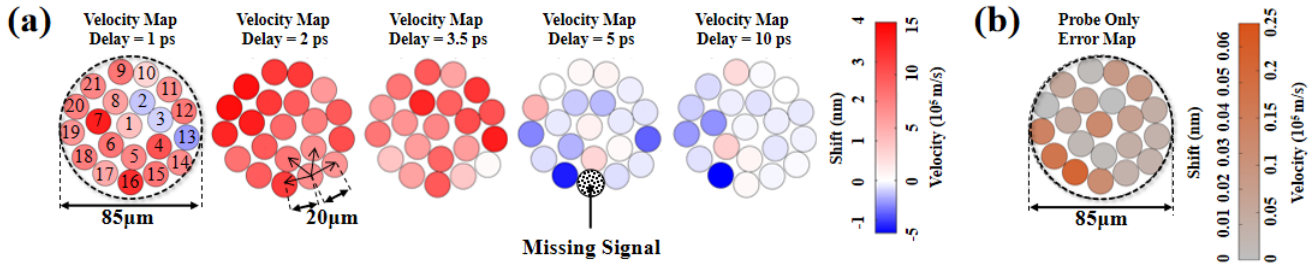


FIG. 7. (a) Reconstructed velocity maps on each plasma location as a function of laser delay. (b) Probe beam only error map.

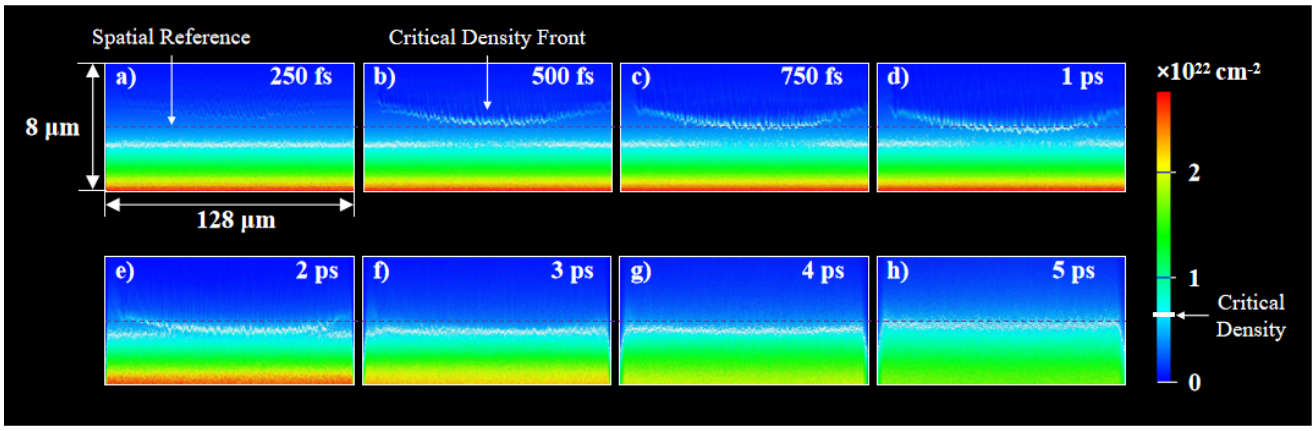


FIG. 8. Simulated evolution of the plasma surface density in a $SiO_2$ target irradiated at an intensity of $1.6\times10^{18}$ W/cm$^2$. The critical density front is presented in white colour.

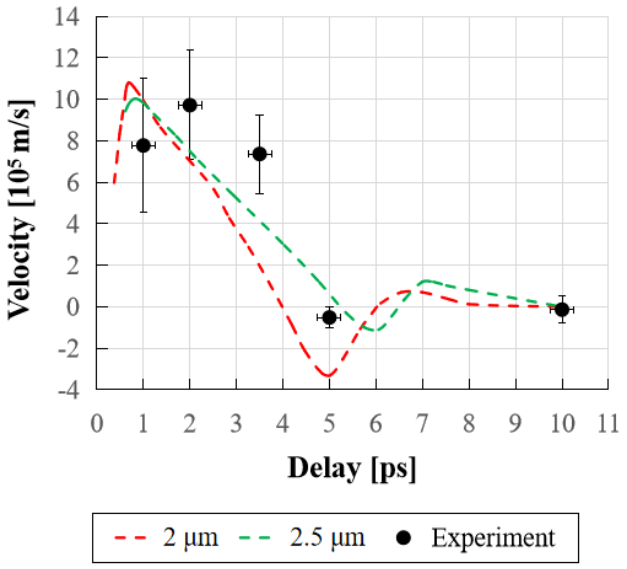


FIG. 9. Measured mean velocities over the entire probed plasma as a function of delay. Dashed lines are EPOCH calculations at the real experiment conditions for a pre-plasma scale length of 2 and 2.5 $\mu$m.

require further investigation, but the major candidates could be Raleigh-Taylor and Weibel instabilities. This might leads to the local variations in the measured velocity map.

## VI. CONCLUSION AND OUTLOOK

We developed and tested a flexible multichannel fiber-based imaging spectrometer (FISER) that uses a single spectrometer to spatio-temporally resolve the velocity of the critical surface in laser created plasmas. This plasma diagnostic is applicable to high repetition-rates, only limited by targetry and camera readout time. The analysed data allowed us to generate spatio-temporal maps of laser-driven hot plasmas generated by femtosecond pulses with intensities of the order $10^{18}$ W/cm$^2$). The number of fibers can be increased (to e.g. 100) to provide higher resolution maps while keeping the same field of view.

## ACKNOWLEDGMENT

This work was performed under the auspices of the (U.S.) Department of Energy (DOE) under Grant No. STTR DE-SC0022935 using facilities supported by LaserNet US under US Department of Energy Fusion Energy Sciences grant US DE-SC0021246. JJR acknowledges support from a DoD Vannevar Bush Faculty Fellowship, ONR award N000142012842

## AUTHOR DECLARATIONS

### Conflict of Interest

The authors have no conflicts to disclose.

## DATA AVAILABILITY

The data that support the findings of this study are available from the corresponding author upon reasonable request.

## REFERENCES


[1]C. N. Danson, C. Haefner, J. Bromage, T. Butcher, J.-C. F. Chanteloup, E. A. Chowdhury, A. Galvanauskas, L. A. Gizzi, J. Hein, D. I. Hillier, and et al., "Petawatt and exawatt class lasers worldwide," High Power Laser Science and Engineering **7**, e54 (2019).

[2]K. U. Akli, S. B. Hansen, A. J. Kemp, R. R. Freeman, F. N. Beg, D. C. Clark, S. D. Chen, D. Hey, S. P. Hatchett, K. Highbarger, E. Giraldez, J. S. Green, G. Gregori, K. L. Lancaster, T. Ma, A. J. MacKinnon, P. Norreys, N. Patel, J. Pasley, C. Shearer, R. B. Stephens, C. Stoeckl, M. Storm, W. Theobald, L. D. Van Woerkom, R. Weber, and M. H. Key, "Laser heating of solid matter by light-pressure-driven shocks at ultrarelativistic intensities," Phys. Rev. Lett. **100**, 165002 (2008).

[3]B. F. Kraus, L. Gao, K. W. Hill, M. Bitter, P. C. Efthimion, T. A. Gomez, A. Moreau, R. Hollinger, S. Wang, H. Song, J. J. Rocca, and R. C. Mancini, "Solid-density ion temperature from redshifted and double-peaked stark line shapes," Phys. Rev. Lett. **127**, 205001 (2021).

[4]R. Hollinger, S. Wang, Y. Wang, A. Moreau, M. G. Capeluto, H. Song, A. Rockwood, E. Bayarsaikhan, V. Kaymak, A. Pukhov, V. N. Shlyaptsev, and J. J. Rocca, "Extreme ionization of heavy atoms in solid-density plasmas by relativistic second-harmonic laser pulses," Nature Photonics **14**, 607–611 (2020).

[5]S. Palaniyappan, B. M. Hegelich, Y. Wang, A. Moreau, M. G. Capeluto, H.-C. Wu, D. Jung, D. C. Gautier, L. Yin, B. J. Albright, R. P. Johnson, T. Shimada, S. Letzring, D. T. Offermann, J. Ren, C. Huang, R. Horlein, B. Dromey, J. C. Fernandez, and R. C. Shah, "Dynamics of relativistic transparency and optical shuttering in expanding overdense plasmas," Nature Physics **8**, 763–769 (2012).

[6]M. Roth, D. Jung, K. Falk, N. Guler, O. Deppert, M. Devlin, A. Favalli, J. Fernandez, D. Gautier, M. Geissel, R. Haight, C. E. Hamilton, B. M. Hegelich, R. P. Johnson, F. Merrill, G. Schaumann, K. Schoenberg, M. Schollmeier, T. Shimada, T. Taddeucci, J. L. Tybo, F. Wagner, S. A. Wender, C. H. Wilde, and G. A. Wurden, "Bright laser-driven neutron source based on the relativistic transparency of solids," Phys. Rev. Lett. **110**, 044802 (2013).

[7]A. Y. Faenov, J. Colgan, S. B. Hansen, A. Zhidkov, T. A. Pikuz, M. Nishiuchi, S. A. Pikuz, I. Y. Skobelev, J. Abdallah, H. Sakaki, A. Sagisaka, A. S. Pirozhkov, K. Ogura, Y. Fukuda, M. Kanasaki, N. Hasegawa, M. Nishikino, M. Kando, Y. Watanabe, T. Kawachi, S. Masuda, T. Hosokai, R. Kodama, and K. Kondo, "Nonlinear increase of x-ray intensities from thin foils irradiated with a 200 tw femtosecond laser," Scientific Reports **5**, 13436 (2015).

[8]R. Hollinger, C. Bargsten, V. N. Shlyaptsev, V. Kaymak, A. Pukhov, M. G. Capeluto, S. Wang, A. Rockwood, Y. Wang, A. Townsend, A. Prieto, P. Stockton, A. Curtis, and J. J. Rocca, "Efficient picosecond x-ray pulse generation from plasmas in the radiation dominated regime," Optica **4**, 1344–1349 (2017).

[9]H. Chen, S. C. Wilks, D. D. Meyerhofer, J. Bonlie, C. D. Chen, S. N. Chen, C. Courtois, L. Elberson, G. Gregori, W. Kruer, O. Landoas, J. Mithen, J. Myatt, C. D. Murphy, P. Nilson, D. Price, M. Schneider, R. Shepherd, C. Stoeckl, M. Tabak, R. Tommasini, and P. Beiersdorfer, "Relativistic quasi-monoenergetic positron jets from intense laser-solid interactions," Phys. Rev. Lett. **105**, 015003 (2010).

[10]A. Higginson, R. J. Gray, M. King, R. J. Dance, R. Wilson, R. Capdessus, C. Armstrong, J. S. Green, S. J. Hawkes, P. Martin, W. Q. Wei, S. R. Mirfayzi, X. H. Yuan, S. Kar, M. Borghesi, R. J. Clarke, D. Neely, and P. McKenna, "Near-100 mev protons via a laser-driven transparencyenhanced hybrid acceleration scheme," Nature Communications **9**, 724 (2018).

[11]J. J. Honrubia and J. M. ter Vehn, "Fast ignition of fusion targets by laser-driven electrons*," Plasma Physics and Controlled Fusion **51**, 014008 (2008).

[12]S. Eliezer, H. Hora, G. Korn, N. Nissim, and J. M. Martinez Val, "Avalanche proton-boron fusion based on elastic nuclear collisions," Physics of Plasmas **23**, 050704 (2016).

[13]M. Nallaperumal, G. N. Namboodiri, and T. Roy, "Neutron imaging for aerospace applications," in Neutron Imaging: Basics, Techniques and Applications, edited by D. K. Aswal, P. S. Sarkar, and Y. S. Kashyap (Springer Singapore, Singapore, 2022) pp. 237–252.

[14]M. Zawisky, M. Bastürk, J. Rehacek, and Z. Hradil, "Neutron tomographic investigations of boron-alloyed steels," Journal of Nuclear Materials **327**, 188–193 (2004).

[15]H. Y. Tan, C. H. Yeong, Y. H. Wong, M. McKenzie, A. Kasbollah, M. N. Md. Shah, and A. C. Perkins, "Neutron-activated theranostic radionuclides for nuclear medicine," Nuclear Medicine and Biology **90-91**, 55–68 (2020).

[16]L. M. Barker and R. E. Hollenbach, "Laser interferometer for measuring high velocities of any reflecting surface," Journal of Applied Physics **43**, 4669–4675 (1972).

[17]P. M. Celliers, D. K. Bradley, G. W. Collins, D. G. Hicks, T. R. Boehly, and W. J. Armstrong, "Line-imaging velocimeter for shock diagnostics at the omega laser facility," Review of Scientific Instruments **75**, 4916–4929 (2004).

[18]C. F. Burrell, W. S. Cooper, R. R. Smith, and W. F. Steele, "Doppler shift spectroscopy of powerful neutral beams," Review of Scientific Instruments **51**, 1451–1462 (1980).

[19]T. Dewandre, J. R. Albritton, and E. A. Williams, "Doppler shift of laser light reflected from expanding plasmas," The Physics of Fluids **24**, 528-536 (1981).

[20]J. Khachan and S. Collis, "Measurements of ion energy distributions by doppler shift spectroscopy in an inertial-electrostatic confinement device," Physics of Plasmas **8**, 1299–1304 (2001).

[21]K. Jana, A. D. Lad, D. West, W. Trickey, C. Underwood, Y. M. Ved, A. P. L. Robinson, J. Pasley, and G. R. Kumar, "Femtosecond, two-dimensional spatial doppler mapping of ultraintense laser-solid target interaction," Phys. Rev. Res. **3**, 033034 (2021).

[22]K. Jana, A. D. Lad, A. Dulat, Y. M. Ved, and G. R. Kumar, "Ultrafast time-resolved two-dimensional velocity mapping of the hot-dense plasmas generated by intense-laser pulses," AIP Advances **12**, 095112 (2022).

[23]A. Gjurchinovski, "The doppler effect from a uniformly moving mirror," European Journal of Physics **26**, 643 (2005).

[24]Y. Wang, S. Wang, A. Rockwood, B. M. Luther, R. Hollinger, A. Curtis, C. Calvi, C. S. Menoni, and J. J. Rocca, "0.85 pw laser operation at 3.3 hz and high-contrast ultrahigh-intensity $\lambda$ = 400 nm second-harmonic beamline," Opt. Lett. **42**, 3828–3831 (2017).

[25]T. D. Arber, K. Bennett, C. S. Brady, A. Lawrence-Douglas, M. G. Ramsay, N. J. Sircombe, P. Gillies, R. G. Evans, H. Schmitz, A. R. Bell, and C. P. Ridgers, "Contemporary particle-in-cell approach to laser-plasma modelling," Plasma Physics and Controlled Fusion **57**, 113001 (2015).

[26]A. Y. V., V. P. Avtonomov, N. G. Basov, G. Korn, G. V. Sklizkov, and V. N. Shlyaptsev, "Contemporary particle-in-cell approach to laser-plasma modelling," Journal of Soviet Laser Research **10**, 1573–8760 (1989).